J Electr Eng Technol Vol. 8, No. 5: 1086-1095, 2013
http://dx.doi.org/10.5370/JEET.2013.8.5.1086

ISSN(Print) 1975-0102
ISSN(Online) 2093-7423

Analysis and Modeling of Parallel Three-Phase Boost Converters Using Three-Phase Coupled Inductor

Chang-Soon Lim*, Kui-Jun Lee, Rae-Young Kim* and Dong-Seok Hyun†**

Abstract – The main issue of parallel three-phase boost converters is reduction of the low- and high frequency circulating currents. Most present technologies concentrate on low frequency circulating current because the circulating current controller cannot mitigate the high frequency circulating current. In this paper, analytical approach of three-phase coupled inductor applied to parallel system becomes an important objective to effectively reduce the low- and high frequency circulating currents. The characteristics of three-phase coupled inductor based on a structure and voltage equations are mathematically derived. The modified voltage equations are then applied to parallel three-phase boost converters to develop averaged models in stationary coordinates and rotating coordinates. Based on the averaged modeling approach, design of the circulating current controller is presented. Simulation and experimental results demonstrate the effectiveness of the analysis and modeling for the parallel three-phase boost converters using three-phase coupled inductor.

Keywords: Parallel three-phase boost converters, Circulating current, Three-phase coupled inductor.

1. Introduction

Parallel three-phase boost converters have many advantages, such as high power under a lower voltage or current ripple, easy modularity, fast-dynamic response, and high efficiency. Therefore, their utilization has dramatically increased in various applications including uninterruptible power supplies (UPS), motor drives, and power factor correction (PFC) equipment [1-3].

However, one of the major concerns with parallel three-phase boost converters is the reduction of the low- and high frequency circulating currents. A low frequency circulating current may be present in the case of small unbalances between two converters, such as different line inductances or different duty cycles. A high frequency circulating current occurs when the interleaved PWM is applied to the parallel three-phase boost converters.

A straightforward solution for the low- and high frequency circulating currents is to disrupt the circulating current path. This is easily achieved using a transformer or separate power supplies on the AC side [4-5]. This solution results in an overall system which is heavy, bulky, and high-priced. To avoid these issues, several circulating current controllers which do not require installation of additional hardware have been proposed for the low frequency circulating current [6-8]. However, these controllers are unable to mitigate the high frequency circulating current due to its identical bandwidth to the switching frequency. In order to reduce the high frequency circulating current, installation of additional system hardware is unavoidable.

Recently, various methods using the winding-coupled inductor have been presented to achieve performance improving results [9-12]. In order to effectively reduce low- and high frequency circulating current, this paper analyzes three-phase coupled inductor applied to parallel three-phase boost converters, as shown in Fig. 1.

In Section 2, the characteristics of three-phase coupled inductor connected to three-phase AC source are mathe-

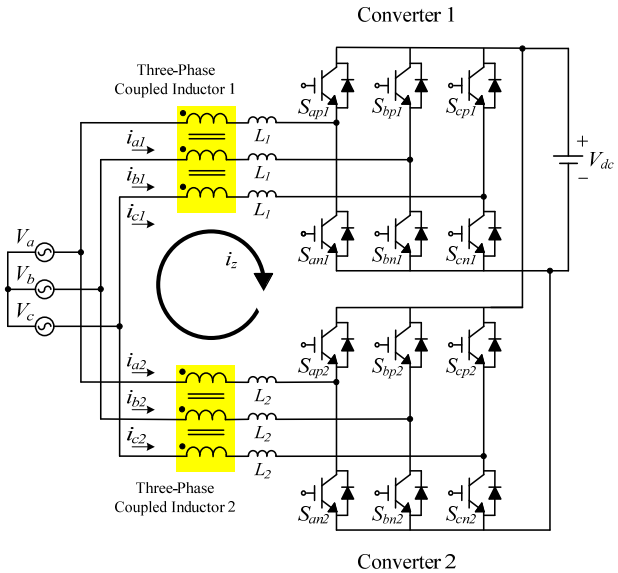

Fig. 1. Parallel three-phase boost converters including three-phase coupled inductor

† Corresponding Author: Dept. of Electrical Engineering, Hanyang University, Korea. (dshyun@hanyang.ac.kr)
* Dept. of Electrical Engineering, Hanyang University, Korea. ({dreamdepot, rykim}@hanyang.ac.kr)
** FREEDM Systems Center, North Carolina State University, USA. (kuijun.lee@gmail.com)
Received: December 8, 2012; Accepted: April 18, 2013

matically derived by a structure and voltage equations. Then, the modified voltage equation of three-phase coupled inductor is presented. Section 3 introduces averaged models, which can simultaneously reduce low- and high frequency circulating currents, in stationary coordinates and rotating coordinates. Based on the averaged modeling approach, section 4 presents design of circulating current controller for parallel three-phase boost converters using three-phase coupled inductor. Section 5 shows simulation and experimental results to demonstrate the effectiveness of the analysis and modeling approach. Section 6 summarizes the major contributions of this paper.

2. Analysis of the Three-Phase Coupled Inductor

This section analyzes the three-phase coupled inductor in parallel three-phase boost converters. The three-phase coupled inductor structure is used to examine how the three-phase coupled inductor mitigates the circulating current. Subsequently, voltage equations of the three-phase coupled inductor are examined to model parallel three-phase boost converters including the three-phase coupled inductor.

2.1 Three-phase coupled inductor structure

Fig. 2 shows a three-phase coupled inductor (i.e., the three-winding integrated magnetic device) structure with reference directions for the currents when three-phase currents i_a, i_b, and i_c flow through winding N. In the three-phase coupled inductor, the three total flux equations are

$$\phi_a = \phi_{aa} + \phi_{ba} + \phi_{ca} = \rho_{aa} N i_a + \rho_{ba} N i_a + \rho_{ca} N i_a \quad (1)$$

$$\phi_b = \phi_{ab} + \phi_{bb} + \phi_{cb} = \rho_{ab} N i_b + \rho_{bb} N i_b + \rho_{cb} N i_b \quad (2)$$

$$\phi_c = \phi_{ac} + \phi_{bc} + \phi_{cc} = \rho_{ac} N i_c + \rho_{bc} N i_c + \rho_{cc} N i_c \quad (3)$$

where φ_x is the total flux linking coil x in the three-phase coupled inductor, φ_{xx} is the flux linking coil x produced by a current in coil x in the three-phase coupled inductor, φ_{yx} is the flux linking coil y produced by a current in coil x in the three-phase coupled inductor, ρ_{xx} is the permeance of the space occupied by the flux φ_{xx} in the three-phase coupled inductor, and ρ_{yx} is the permeance of the space occupied by the flux φ_{yx} in the three-phase coupled inductor.

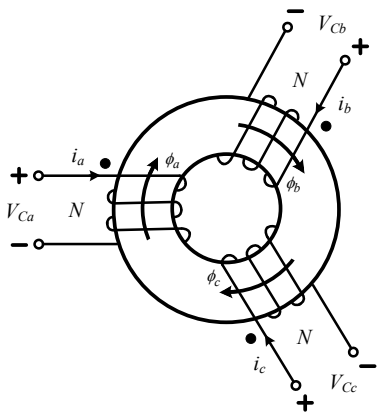

Fig. 2. Simplified structure of the three-phase coupled inductor

If the coupled inductor is in an ideal state, it is possible to assume the following:

$$\rho_s = \rho_{aa} = \rho_{bb} = \rho_{cc} = 0 \quad (4)$$

$$\rho_m = \rho_{ab} = \rho_{ac} = \rho_{ba} = \rho_{bc} = \rho_{ca} = \rho_{cb} \quad (5)$$

Summing up (1-3), and using (4-5), the following equation can be derived:

$$\phi_a + \phi_b + \phi_c = 2\rho_m N(i_a + i_b + i_c) \quad (6)$$

Eq. (6) indicates that the net magnetic flux in the core is nearly zero under balanced condition. However, under unbalanced conditions, the net magnetic flux in the core is non-zero. Specifically, if there is no circulating current, the system is not influenced by the three-phase coupled inductor.

2.2 Voltage equations for three-phase coupled inductor

The voltage equations for a three-phase coupled inductor are typically defined as

$$V_a = L_{aa}\frac{d}{dt}i_a + L_{ab}\frac{d}{dt}i_b + L_{ac}\frac{d}{dt}i_c \quad (7)$$

$$V_b = L_{ba}\frac{d}{dt}i_a + L_{bb}\frac{d}{dt}i_b + L_{bc}\frac{d}{dt}i_c \quad (8)$$

$$V_c = L_{ca}\frac{d}{dt}i_a + L_{cb}\frac{d}{dt}i_b + L_{cc}\frac{d}{dt}i_c \quad (9)$$

where L_{xx} is the self-inductance produced by a current in coil x in the three-phase coupled inductor, and L_{yx} is the mutual inductance produced by a current in coil x in the three-phase coupled inductor.

Similar to (4-5), the self-inductance and mutual inductance can be respectively assumed to be

$$L_s = L_{aa} = L_{bb} = L_{cc} \quad (10)$$

$$L_m = L_{ab} = L_{ac} = L_{ba} = L_{bc} = L_{ca} = L_{cb} \quad (11)$$

Therefore, the relationship between self-inductance and mutual inductance can be expressed as

$$L_m = k_c\sqrt{L_s \cdot L_s} = k_c \cdot L_s \quad (12)$$

where k_c is the coupling coefficient in the three-phase coupled inductor.

In Fig. 1, the circulating current i_z is defined as

$$i_z = i_{z1} = i_{a1} + i_{b1} + i_{c1} = -i_{z2} = -(i_{a2} + i_{b2} + i_{c2}) \quad (13)$$

Using (10-13), three-phase coupled inductor voltage Eqs. (7-9) can be rewritten as

$$V_a = L_s(1-k_c)\frac{d}{dt}i_a + k_c \cdot L_s \frac{d}{dt}i_z \quad (14)$$

$$V_b = L_s(1-k_c)\frac{d}{dt}i_b + k_c \cdot L_s \frac{d}{dt}i_z \quad (15)$$

$$V_c = L_s(1-k_c)\frac{d}{dt}i_c + k_c \cdot L_s \frac{d}{dt}i_z \quad (16)$$

where L_S (1 - k_c) and $k_c \cdot L_S$ are the leakage inductance to the line current and the mutual inductance to the circulating current, respectively.

The modified voltage Eqs. (14-16) indicate that the leakage inductance and mutual inductance are dependent on the coupling coefficient of the three-phase coupled inductor. In other words, the mutual inductance to the circulating current is increased and leakage inductance to the line current is decreased if the coupling coefficient k_c is increased.

3. Averaged Modeling

Generally, a traditional modeling approach for a three-phase boost converter is to transform three-phase stationary coordinates into synchronous rotating coordinates. In this case, the zero-sequence component does not influence the input line currents or the output direct current (DC) voltages because there is no zero-sequence component.

However, the traditional modeling approach cannot be used for parallel three-phase boost converters because zero-sequence components do exist. Therefore, in order to model the zero-sequence components in parallel three-phase boost converters, an averaged model based on a phase-leg averaging technique was used in [6] and [13].

In order to predict the system dynamics and design controller, three models (averaged model in stationary coordinates, average model in rotating coordinates, and small-signal model) for parallel three-phase boost converters including the three-phase coupled inductor will be described in this section. As shown in Fig. 3, the three stages are needed in order to obtain linear time invariant (LTI) model: phase-leg averaging technique, abc/dqz transformation, and perturbation and linearization.

3.1 Averaged model in stationary coordinates

In order to accurately reflect a three-phase coupled inductor to parallel three-phase boost converters model, modified voltage Eqs. (14-16) are added to conventional averaged model in stationary coordinate. As a result, the

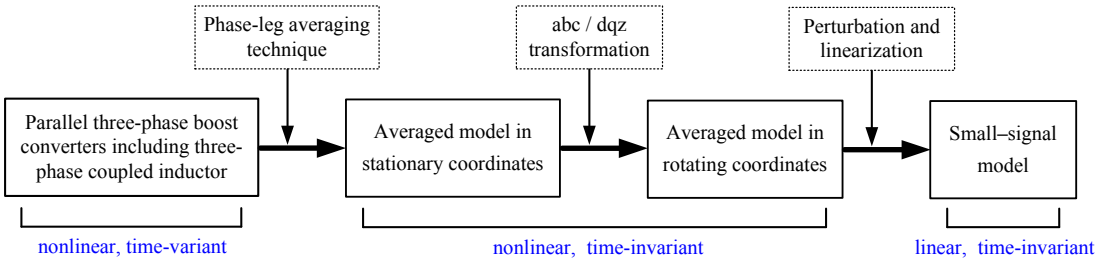

Fig. 3. The relationship of three modeling methods.

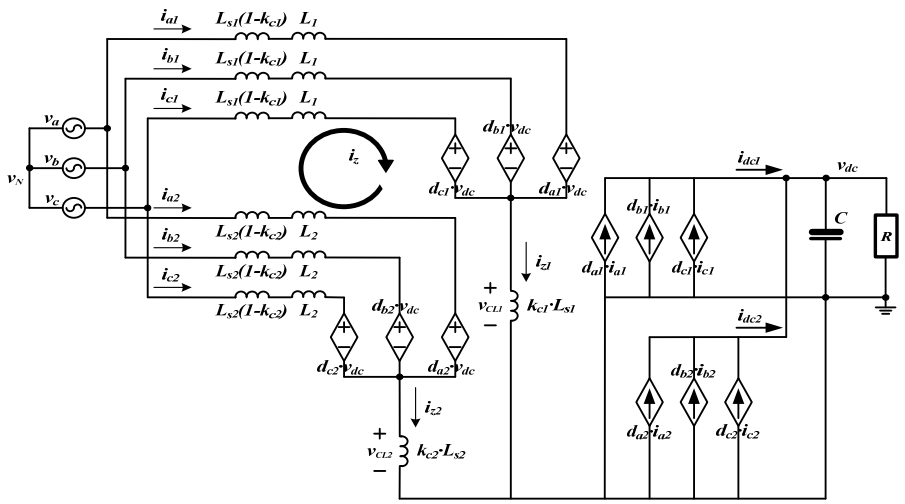

Fig. 4. Averaged model of parallel three-phase boost converters including the three-phase coupled inductor in stationary coordinates.

averaged model of parallel three-phase boost converters including three-phase coupled inductor in stationary coordinate is proposed, as shown in Fig. 4.

This model can simultaneously reduce the low and high frequency circulating currents. Using the Fig. 4, the state-space equations in stationary coordinates can be easily obtained:

$$\frac{d}{dt}\begin{bmatrix} i_{a1} \\ i_{b1} \\ i_{c1} \end{bmatrix} = \frac{1}{L_1 + L_{s1}(1-k_{c1})}\begin{bmatrix} v_{aN} + v_N - v_{CL1} \\ v_{bN} + v_N - v_{CL1} \\ v_{cN} + v_N - v_{CL1} \end{bmatrix} - \frac{v_{dc}}{L_1 + L_{s1}(1-k_{c1})}\begin{bmatrix} d_{a1} \\ d_{b1} \\ d_{c1} \end{bmatrix} \tag{17}$$

$$\frac{d}{dt}\begin{bmatrix} i_{a2} \\ i_{b2} \\ i_{c2} \end{bmatrix} = \frac{1}{L_2 + L_{s2}(1-k_{c2})}\begin{bmatrix} v_{aN} + v_N - v_{CL2} \\ v_{bN} + v_N - v_{CL2} \\ v_{cN} + v_N - v_{CL2} \end{bmatrix} - \frac{v_{dc}}{L_2 + L_{s2}(1-k_{c2})}\begin{bmatrix} d_{a2} \\ d_{b2} \\ d_{c2} \end{bmatrix} \tag{18}$$

$$\frac{d}{dt}v_{dc} = \frac{1}{C}\left(\begin{bmatrix} d_{a1} & d_{b1} & d_{c1} \end{bmatrix}\cdot\begin{bmatrix} i_{a1} \\ i_{b1} \\ i_{c1} \end{bmatrix} + \begin{bmatrix} d_{a2} & d_{b2} & d_{c2} \end{bmatrix}\cdot\begin{bmatrix} i_{a2} \\ i_{b2} \\ i_{c2} \end{bmatrix}\right) - \frac{v_{dc}}{RC} \tag{19}$$

where V_{CL1} and V_{CL2} are

$$v_{CL1} = k_{c1}L_{s1}\frac{d}{dt}i_{z1} \qquad v_{CL2} = k_{c2}L_{s2}\frac{d}{dt}i_{z2}$$

and

d_a d_b d_c duty cycle for three-phase
i_a i_b i_c averaged three-phase currents during one switching period

3.2 Averaged model in rotating coordinates

In order to reduce steady-state error, the model in the stationary coordinates is usually transformed into rotating coordinates. The transformation matrix T is defined as follows:

$$T = \sqrt{\frac{2}{3}}\begin{bmatrix} \cos\omega t & \cos(\omega t - \frac{2\pi}{3}) & \cos(\omega t + \frac{2\pi}{3}) \\ -\sin\omega t & -\sin(\omega t - \frac{2\pi}{3}) & -\sin(\omega t + \frac{2\pi}{3}) \\ \frac{1}{\sqrt{2}} & \frac{1}{\sqrt{2}} & \frac{1}{\sqrt{2}} \end{bmatrix} \tag{20}$$

where ω is angular frequency.

The variables in the stationary coordinates Y_{abc} can be transformed into the rotating coordinates Y_{dqz} by using transformation matrix (20).

$$Y_{dqz} = T \cdot Y_{abc} \tag{21}$$

Applying Eqs. (21) to (17-19), the state-space equations in rotating coordinates can be defined as

$$\frac{d}{dt}\begin{bmatrix} i_{d1} \\ i_{q1} \\ i_{z1} \end{bmatrix} = \frac{1}{L_1 + L_{s1}(1-k_{c1})}\begin{bmatrix} v_d \\ v_q \\ v_z + 3(v_N - v_{CL1}) \end{bmatrix} - \begin{bmatrix} 0 & -\omega & 0 \\ \omega & 0 & 0 \\ 0 & 0 & 0 \end{bmatrix}\cdot\begin{bmatrix} i_{d1} \\ i_{q1} \\ i_{z1} \end{bmatrix} - \frac{v_{dc}}{L_1 + L_{s1}(1-k_{c1})}\begin{bmatrix} d_{d1} \\ d_{q1} \\ d_{z1} \end{bmatrix} \tag{22}$$

$$\frac{d}{dt}\begin{bmatrix} i_{d2} \\ i_{q2} \\ i_{z2} \end{bmatrix} = \frac{1}{L_2 + L_{s2}(1-k_{c2})}\begin{bmatrix} v_d \\ v_q \\ v_z + 3(V_N - V_{CL2}) \end{bmatrix} - \begin{bmatrix} 0 & -\omega & 0 \\ \omega & 0 & 0 \\ 0 & 0 & 0 \end{bmatrix}\cdot\begin{bmatrix} i_{d2} \\ i_{q2} \\ i_{z2} \end{bmatrix} - \frac{v_{dc}}{L_2 + L_{s2}(1-k_{c2})}\begin{bmatrix} d_{d2} \\ d_{q2} \\ d_{z2} \end{bmatrix} \tag{23}$$

$$\frac{d}{dt}v_{dc} = \frac{1}{C}\left(\begin{bmatrix} d_{d1} & d_{q1} & \frac{d_{z1}}{3} \end{bmatrix}\cdot\begin{bmatrix} i_{d1} \\ i_{q1} \\ i_{z1} \end{bmatrix} + \begin{bmatrix} d_{d2} & d_{q2} & \frac{d_{z2}}{3} \end{bmatrix}\cdot\begin{bmatrix} i_{d2} \\ i_{q2} \\ i_{z2} \end{bmatrix}\right) - \frac{v_{dc}}{RC} \tag{24}$$

where d_{z1} and d_{z2} are

$$d_{z1} = d_{a1} + d_{b1} + d_{c1}, \quad d_{z2} = d_{a2} + d_{b2} + d_{c2}$$

Using the Eq. (13), the state-space Eqs. (22-24) can be rewritten as

$$\frac{d}{dt}\begin{bmatrix} i_{d1} \\ i_{q1} \end{bmatrix} = \frac{1}{L_1 + L_{s1}(1-k_{c1})}\begin{bmatrix} v_d \\ v_q \end{bmatrix} - \begin{bmatrix} 0 & -\omega \\ \omega & 0 \end{bmatrix}\cdot\begin{bmatrix} i_{d1} \\ i_{q1} \end{bmatrix} - \frac{v_{dc}}{L_1 + L_{s1}(1-k_{c1})}\begin{bmatrix} d_{d1} \\ d_{q1} \end{bmatrix} \tag{25}$$

$$\frac{d}{dt}\begin{bmatrix} i_{d2} \\ i_{q2} \end{bmatrix} = \frac{1}{L_2 + L_{s2}(1-k_{c2})}\begin{bmatrix} v_d \\ v_q \end{bmatrix} - \begin{bmatrix} 0 & -\omega \\ \omega & 0 \end{bmatrix}\cdot\begin{bmatrix} i_{d2} \\ i_{q2} \end{bmatrix} - \frac{v_{dc}}{L_2 + L_{s2}(1-k_{c2})}\begin{bmatrix} d_{d2} \\ d_{q2} \end{bmatrix} \tag{26}$$

$$\frac{d}{dt}i_Z = -\frac{(d_{z1} - d_{z2})\cdot v_{dc}}{L_1 + L_2 + L_{s1}(1+2k_{c1}) + L_{s2}(1+2k_{c2})} \tag{27}$$

$$\frac{d}{dt}v_{dc} = \frac{1}{C}(\begin{bmatrix} d_{d1} & d_{q1} \end{bmatrix}\cdot\begin{bmatrix} i_{d1} \\ i_{q1} \end{bmatrix} + \begin{bmatrix} d_{d2} & d_{q2} \end{bmatrix}\cdot\begin{bmatrix} i_{d2} \\ i_{q2} \end{bmatrix} + \frac{(d_{z1}-d_{z2})}{3}i_Z) - \frac{v_{dc}}{RC} \tag{28}$$

Unlike the single three-phase converter system, the parallel three-phase converters system has zero-sequence component as (27) and (28). Using the state-space Eqs. (25-28), the averaged model of parallel three-phase boost converters including the three-phase coupled inductor in rotating coordinates can be developed, as shown in Fig. 5.

3.3 Small-signal model

The averaged Eqs. (25-28) in rotating coordinate are nonlinear functions of the signals in the system. In order to design controller, nonlinear averaged equations must be linearized. Using the averaged small-signal model at a quiescent operating point, the linear model can be easily obtained. In perturbation and linearization step, it is assumed that an averaged values are perturbed by adding the small-signal ac variation ($*$) at a quiescent operating point.

The perturbed value is represented as:

$$\begin{aligned}
&i_{d1} = I_{d1} + i_{d1}^* && i_{q1} = I_{q1} + i_{q1}^* \\
&i_{d2} = I_{d2} + i_{d2}^* && i_{q2} = I_{q2} + i_{q2}^* \\
&i_z = I_z + i_z^* && v_{dc} = V_{dc} + v_{dc}^* \\
&v_d = V_d + v_d^* && v_q = V_q + v_q^* \\
&d_{d1} = D_{d1} + d_{d1}^* && d_{q1} = D_{q1} + d_{q1}^* \\
&d_{d2} = D_{d2} + d_{d2}^* && d_{q2} = D_{q2} + d_{q2}^* \\
&d_{z1} - d_{z2} = \Delta d_z = \Delta D_z + \Delta d_z^*
\end{aligned} \tag{29}$$

Assuming that the input voltage sources are ideal, then

$$v_d^* = v_q^* = 0 \tag{30}$$

The linearization step can be completed by neglecting the nonlinear second-order ac terms because each of the second-order terms is much smaller than the first-order ac terms in magnitude. After the linearization step, the averaged small-signal equation of parallel three-phase boost converters including three-phase coupled inductor can be derived as follows:

$$\frac{d}{dt}X = AX + BU \tag{31}$$

Where

$$A = \begin{bmatrix}
-\frac{1}{RC} & \frac{D_{d1}}{C} & \frac{D_{q1}}{C} & \frac{D_{d2}}{C} & \frac{D_{q2}}{C} & 0 \\
-\frac{D_{d1}}{\alpha} & 0 & \omega & 0 & 0 & 0 \\
-\frac{D_{q1}}{\alpha} & -\omega & 0 & 0 & 0 & 0 \\
-\frac{D_{d2}}{\beta} & 0 & 0 & 0 & \omega & 0 \\
-\frac{D_{q2}}{\beta} & 0 & 0 & -\omega & 0 & 0 \\
0 & 0 & 0 & 0 & 0 & 0
\end{bmatrix} \tag{32}$$

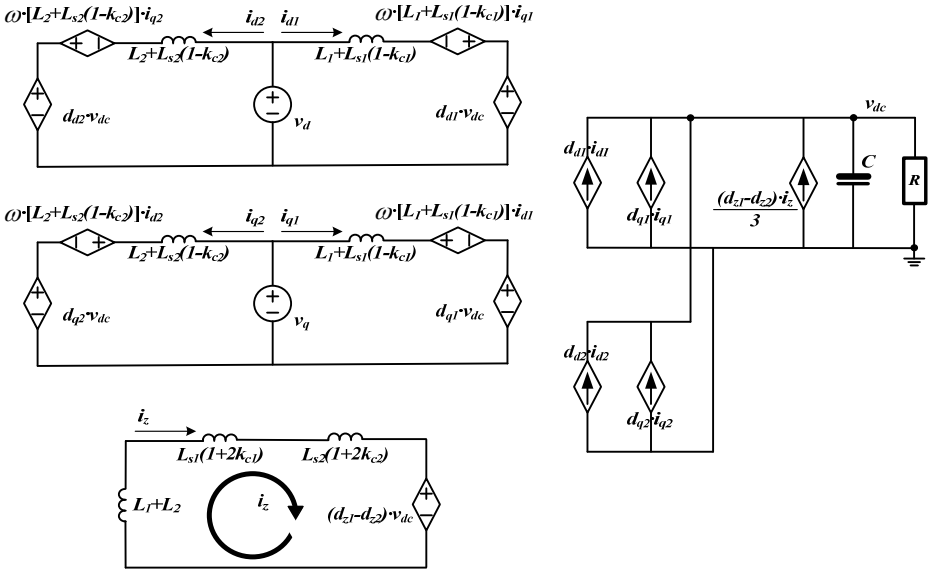

Fig. 5. Averaged model of parallel three-phase boost converters including the three-phase coupled inductor in rotating coordinates.

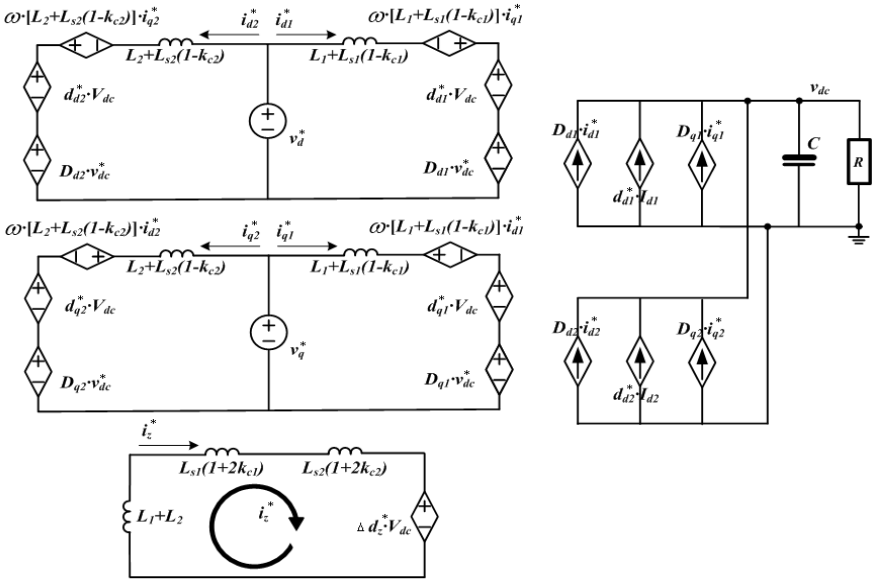

Fig. 6. Averaged small-signal model of parallel three-phase boost converters including three-phase coupled inductor.

$$X = [v_{dc}^* \quad i_{d1}^* \quad i_{q1}^* \quad i_{d2}^* \quad i_{q2}^* \quad i_z^*]^T \tag{33}$$

$$B = \begin{bmatrix} \frac{I_{d1}}{C} & \frac{I_{q1}}{C} & \frac{I_{d2}}{C} & \frac{I_{q2}}{C} & 0 \\ -\frac{V_{dc}}{\alpha} & 0 & 0 & 0 & 0 \\ 0 & -\frac{V_{dc}}{\alpha} & 0 & 0 & 0 \\ 0 & 0 & -\frac{V_{dc}}{\beta} & 0 & 0 \\ 0 & 0 & 0 & -\frac{V_{dc}}{\beta} & 0 \\ 0 & 0 & 0 & 0 & -\frac{V_{dc}}{\gamma} \end{bmatrix} \tag{34}$$

$$U = \begin{bmatrix} d_{d1}^* & d_{q1}^* & d_{d2}^* & d_{q2}^* & \Delta d_z^* \end{bmatrix}^T \tag{35}$$

where α, β, and γ are shown as follows :

$$\alpha = L_1 + L_{s1}(1-k_{c1})$$
$$\beta = L_2 + L_{s2}(1-k_{c2})$$
$$\gamma = L_1 + L_2 + L_{s1}(1+2k_{c1}) + L_{s2}(1+2k_{c2})$$

From the Eq. (31), the averaged small-signal model of parallel three-phase boost converters including three-phase coupled inductor can be developed, as shown in Fig. 6. Since the system model is linearized at a quiescent operating point, the controller for parallel three-phase boost converters including three-phase coupled inductor can be designed.

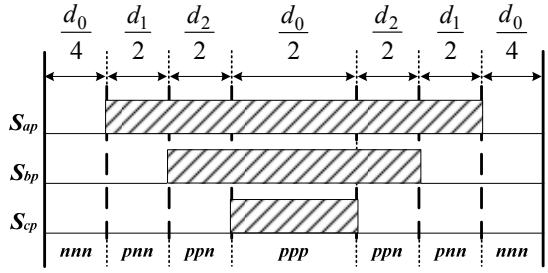

Fig. 7. Relationship between space-vector PWM pattern and duty cycle

4. Design of the Circulating Current Controller

Fig. 7 represents the one space-vector PWM pattern for the three-phase boost converter. d_1, d_2 are duty cycles for active vectors (*pnn* and *ppn*) and d_0 is duty cycle for zero vectors (*ppp* and *nnn*). Therefore, the duty cycles d_a, d_b and d_c of S_{ap}, S_{bp} and S_{cp} can be expressed as

$$d_a = d_{ppp} + d_1 + d_2$$
$$d_b = d_{ppp} + d_2 \qquad d_c = d_{ppp} \tag{36}$$

where d_{ppp} is duty cycle for zero vector (*ppp*).

Since this system consists of two parallel converters, the d_{z1} (converter 1) and d_{z2} (converter 2) are

$$d_{z1} = d_{a1} + d_{b1} + d_{c1} = 3d_{ppp1} + d_{11} + 2d_{21}$$
$$d_{z2} = d_{a2} + d_{b2} + d_{c2} = 3d_{ppp2} + d_{12} + 2d_{22} \tag{37}$$

If two parallel converters have the identical active vectors, Δd_Z^* can be expressed as

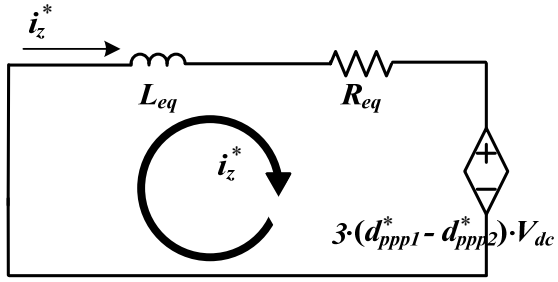

Fig. 8. Simplified zero-sequence dynamic in small-signal model

$$\Delta d_Z^* = d_{Z1}^* - d_{Z2}^* = 3d_{ppp1}^* - 3d_{ppp2}^* \tag{38}$$

As a result, one loop equation for zero-sequence dynamic in Fig. 6 can be rewritten as

$$L_{eq}\cdot\frac{di_z^*}{dt} + R_{eq}\cdot i_z^* = -(3d_{ppp1}^* - 3d_{ppp2}^*)V_{dc} \tag{39}$$

where L_{eq} and R_{eq} are

$$L_{eq} = L_1 + L_2 + L_{s1}(1+2k_{c1}) + L_{s2}(1+2k_{c2})$$
$$R_{eq} = R_{L1} + R_{L2} + R_{C1} + R_{C2} \tag{40}$$

and

R_{L1} R_{L2} Equivalent series resistors of the inductors
R_C R_{C2} Equivalent series resistors of the three-phase coupled inductors

From the Eq. (39), the zero-sequence dynamic of small-signal model is simplified, and is depicted in Fig. 8.

The ac circulating current variation i_z^* can be expressed as the superposition of terms arising from two inputs

$$i_z^* = \frac{3\cdot d_{ppp2}^*\cdot V_{dc}}{L_{eq}\cdot S + R_{eq}} - \frac{3\cdot d_{ppp1}^*\cdot V_{dc}}{L_{eq}\cdot S + R_{eq}} \tag{41}$$

A single circulating current controller is sufficient for controlling the low frequency circulating current since there is only one circulating current. Therefore, the block diagram of the circulating current controller can be developed, as shown in Fig. 9. The transfer function G_1 and G_2 are

$$G_1 = \frac{3\cdot V_{dc}}{L_{eq}\cdot S + R_{eq}} \qquad G_2 = -\frac{3\cdot V_{dc}}{L_{eq}\cdot S + R_{eq}} \tag{42}$$

The PI compensator of (43) is used for the circulating current compensator G_C. Using the circuit parameter:L_1=L_2=2mH, L_{S1}=L_{S2}=1mH, k_{c1}=k_{c2}=0.99, R_{L1}=R_{L2}=0.35Ω, R_{C1}=R_{C2}=0.2Ω, the circulating current compensator parameters are determined. Gain and time constant in Eq.

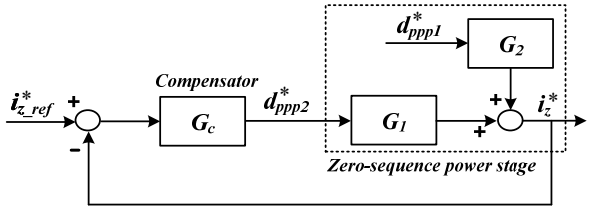

Fig. 9. Block diagram of the circulating current controller in a closed loop

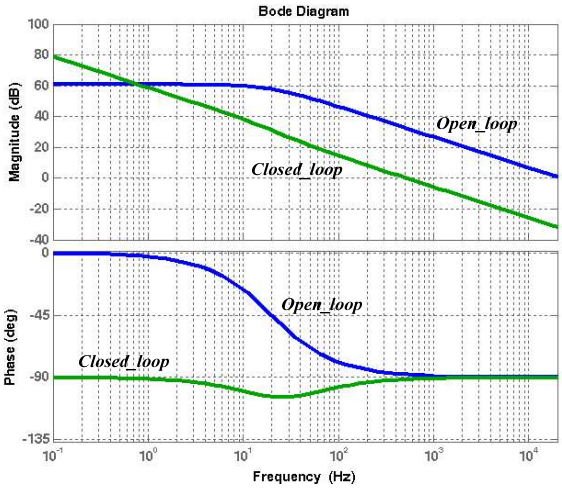

Fig. 10. Magnitude/phase plots of the circulating current controller loop gain for an open and closed loop

(43) are k=0.024 and T=0.0048

$$G_c = k\frac{1+S\cdot T}{S\cdot T} \tag{43}$$

Fig. 10 shows magnitude/phase plots of the circulating current loop gain for an open and closed loop. The compensator design results show a phase margin higher than 85 degree. The crossover frequency is about 500Hz.

5. Simulation and Experimental Results

In order to verify the effectiveness of the analysis and modeling, the prototype specifications in Table 1 were designed, simulated, constructed and experimented. Different line inductance parameters are applied to generate a

Table 1. Parameters for experiment

Parameter	Value
Input line-to-line voltage	220 [V_{rms}]
Output voltage	400 [V]
Output power	3 [kW]
Switching frequency	10 [kHz]
Line inductor, L_1, L_2	2.5 2.0 [mH]
3ϕ coupled inductor, L_{S1}, L_{S2}	1.0 1.0 [mH]
Coefficient of coupling, k_{c1}, k_{c2}	0.99
IGBT modules	BSM200GB120DLC
DSP	TMS320VC33

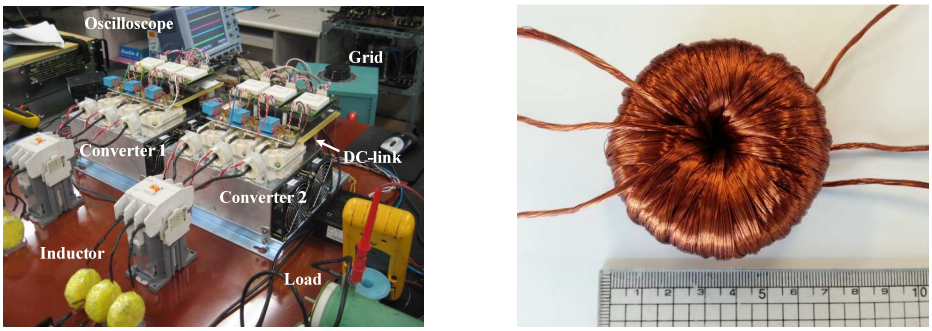

(a) (b)

Fig.11. Photograph of the experimental prototype: (a) Parallel three-phase boost converters; (b) Three-phase coupled inductor.

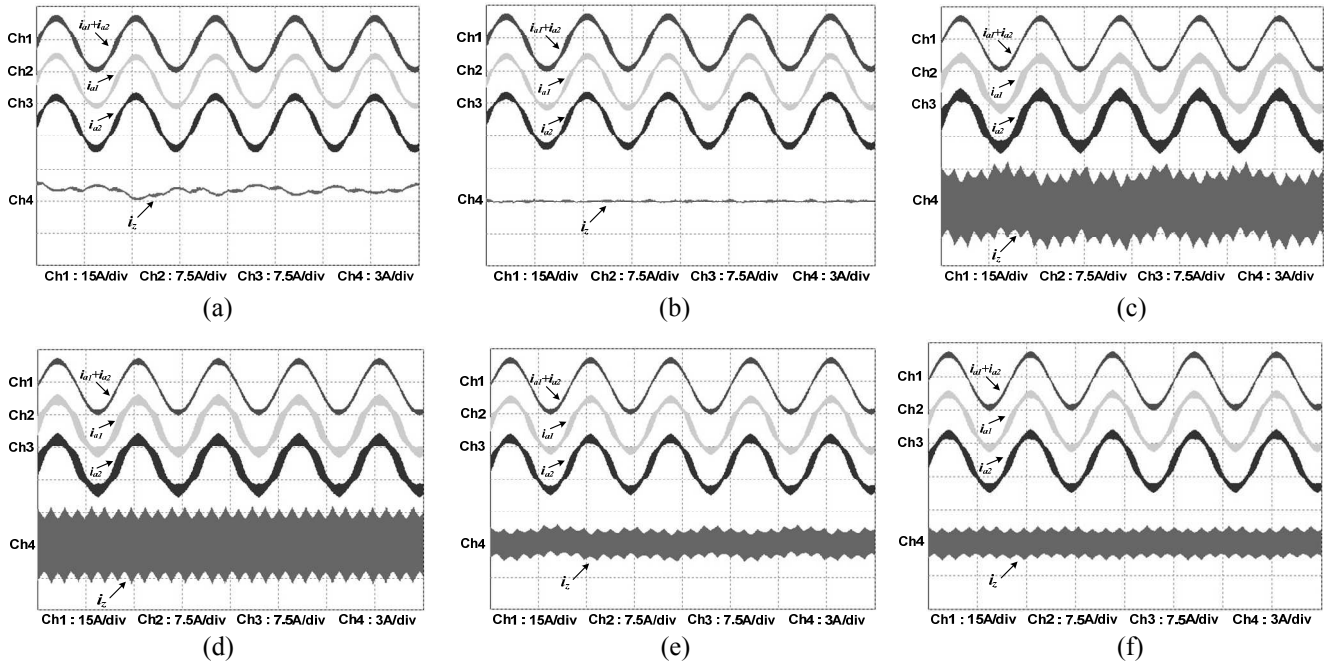

(a) (b) (c)

(d) (e) (f)

Fig. 12. Simulated waveforms of the line currents and the circulating currents: (a) Not use the circulating current controller; (b) Use the circulating current controller; (c) Not use the circulating current controller and the three-phase coupled inductor; (d) Use the only circulating current controller; (e) Use the only three-phase coupled inductor; (f) Use the circulating current controller and the three-phase coupled inductor simultaneously.

low frequency circulating current and a 180-degree interleaved PWM is applied to generate a high frequency circulating current. Figs. 11 (a) and (b) show the test setup of the parallel three-phase boost converters and three-phase coupled inductor, respectively. The power stage consisted of two parallel three-phase boost converters using Infineon IGBT modules, current sensors (ES100C), and isolation amplifiers (AD-202JN), which were used to generate the input line currents and the output DC-link voltage. The control algorithms were programmed and translated into the TMS320VC33 DSP platform.

Fig. 12 shows the simulated waveforms of the line currents and the circulating current in the parallel three-phase boost converters. There is no high frequency circulating current in Fig. 12(a) and (b) since interleaving PWM is not applied for the simulations. Therefore, Fig. 12(b) shows that the low frequency circulating current is effectively reduced by the circulating current controller.

On the other hand, Figs. 12(c) to (f) illustrates simultaneous high frequency and low frequency circulating currents since interleaving PWM is applied in the simulations. As a result, a certain amount of line current (i_{a1}+i_{a2}) ripple is cancelled due to the interleaving PWM, as can be seen by comparing Figs. 12(a) to (b) with Figs. 12(c) to (f). As shown in Fig. 12(d), the circulating current controller only reduces the low frequency circulating current. Both Figs. 12(e) and (f) show that the low frequency and the high frequency circulating currents are reduced by the three-phase coupled inductor. However, the low frequency circulating current shown in Fig. 12(f) is further reduced by applying the circulating current controller.

Fig. 13 shows the experimental waveforms of the line

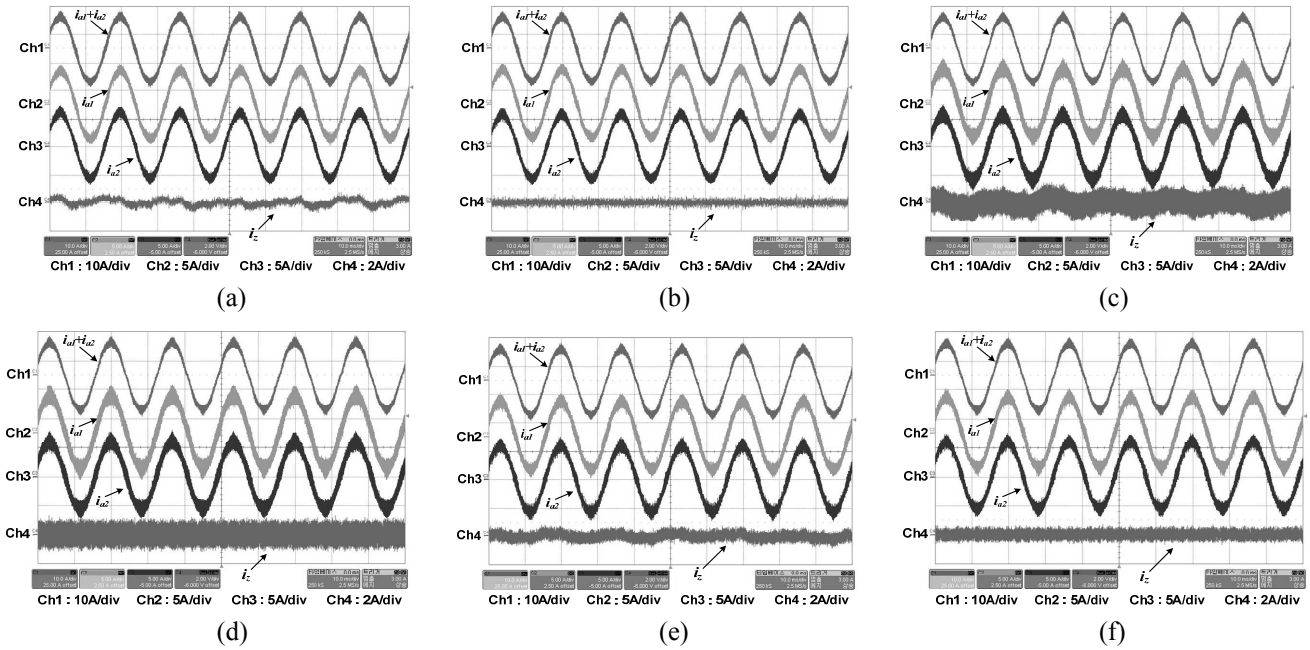

Fig. 13. Experimental waveforms of the line currents and the circulating currents. (a) Not use the circulating current controller. (b) Use the circulating current controller. (c) Not use the circulating current controller and the three-phase coupled inductor. (d) Use the only circulating current controller. (e) Use the only three-phase coupled inductor. (f) Use the circulating current controller and the three-phase coupled inductor simultaneously.

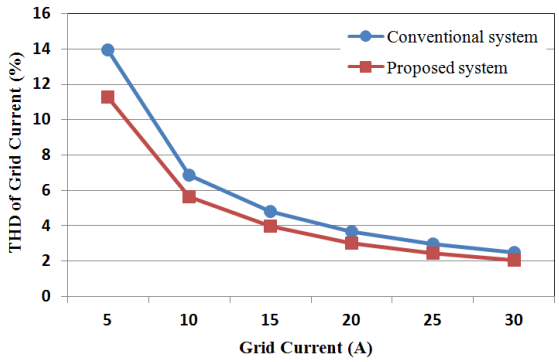

Fig. 14. THD results of the grid currents

currents and the circulating current in the parallel three-phase boost converters. Due to identical conditions and control algorithms, the experimental results were almost similar to the simulated results. Fig. 14 shows the grid current THDs of two different systems. The THD of proposed system is less than the THD of conventional system. Therefore, proposed system can be a good solution to reduce the current harmonic distortion in parallel three-phase boost converters.

6. Conclusion

In this paper, the analysis and modeling of the parallel three-phase boost converters including three-phase coupled inductor was presented to predict system dynamics. To examine the characteristic of three-phase coupled inductor, the structure and voltage equations were mathematically derived. It was shown that the averaged model, which can simultaneously reduce low- and high frequency, was developed in stationary coordinates and rotating coordinates. Based on the averaged modeling approach, the design of the circulating current controller was presented.

Simulation and experimental results demonstrated the effectiveness of three-phase coupled inductor and circulating current controller in parallel three-phase boost converters.

References

[1] K. Xing, F. C. Lee, D. Boroyevich, Z. Ye, and S. K. Mazumder, "The circulating current in paralleled three-phase boost PFC rectifiers," *IEEE Trans. Power Electron.*, Vol. 14, No. 5, pp. 250-256, Sep. 1999

[2] I. Takahashi and M. Yamane, "Multiparallel asymmetrical cycloconverter having improved power factor and waveforms," *IEEE Trans. Ind. Applicat.*, Vol. 22, No. 6, pp. 1007-1016, 1986.

[3] M. Baumann and J. W. Kolar, "Parallel connection of two three-phase three-switch buck-type unity-power-factor rectifier systems with DC-link current balancing," *IEEE Trans. Ind. Electron.*, Vol. 54, No. 6, pp. 3042-3053, Dec. 2007.

[4] T. Kawabata and S. Higashino, "Parallel operation of voltage source inverters," *IEEE Trans. Ind. Applicat.*, Vol. 24, No. 2, pp. 281-287, 1988.

[5] L.-P. Wong, D. K.-W. Cheng, M. H. L. Chow, and Y.-

S. Lee, "Interleaved three-phase forward converter using integrated transformer," *IEEE Trans. Ind. Electron.*, Vol. 52, No. 5, pp. 1246-1260, Oct. 2005.
[6] Z. Ye , D. Boroyevich , J.-Y. Choi and F. C. Lee "Control of circulating current in two parallel three-phase boost rectifiers," IEEE Trans. Power Electron., Vol. 17, pp. 609, Sep. 2002.
[7] K. Xing, F. C. Lee, D. Borojevic, Z. Ye, and S. Mazumder, "Interleaved PWM with discontinuous space-vector modulation," IEEE Trans. Power Electron., Vol. 14, No. 5, pp. 906-917, Sep. 1999.
[8] C.-T. Pan and Y.-H. Liao, "Modeling and coordinate control of circulating current in parallel three-phase boost rectifiers," IEEE Trans. Ind. Electron., Vol. 54, No. 2, pp. 825-838, Apr. 2007.
[9] W. S. Yu, J. -S. Lai, and S. -Y. Park, "An improved zero-voltage switching inverter using two coupled magnetics in one resonant pole," IEEE Trans. Power Electron., Vol. 25, No. 4, pp. 952-961, Apr. 2010.
[10] S.-K. Changchien, T.-J. Liang, J.-F. Chen, and L.-S. Yang, "Novel high step-up dc-dc converter for fuel cell energy conversion system," IEEE Trans. Ind. Electron., Vol. 57, No. 6, pp. 2007-2017, Jun. 2010.
[11] L. Asiminoaei, E. Aeloiza, P. N. Enjeti, and F. Blaabjerg, "Shunt active-power-filter topology based on parallel interleaved inverters," IEEE Trans. Ind. Electron., Vol. 55, No. 3, pp. 1175-1189, Mar. 2008.
[12] B. Yang, W. Li, Y. Zhao, and X. He, "Design and analysis of a gridconnected photovoltaic power system," IEEE Trans. Power Electron., Vol. 25, No. 4, pp. 992-1000, Apr. 2010.
[13] K. Xing, "Modeling, Analysis and Design of Distributed Power Electronics System Based on Building Block Concept," Ph.D. dissertation, Virginia Polytech. Inst. and State Univ., Blacksburg, May 1999.

Chang-Soon Lim He received the B.S. degree in electronic engineering from Soongsil University, Seoul, Korea, in 2009, and the M.S. degree in Electrical Engineering from Hanyang University, Seoul, Korea, in 2011, where he is currently working toward the Ph.D. degree. His research interests include modeling and control of power converter systems, soft switching techniques for renewable energies and battery charger.

Kui-Jun Lee He received the B.S. and Ph.D. degrees in electrical engineering from Hanyang University, Seoul, Korea, in 2005 and 2012, respectively. In 2012, he joined the Future Renewable Electric Energy Delivery and Management (FR-EEDM) Systems Center, North Carolina State University, Raleigh. His research interests include power converter system for renewable energies and soft switching techniques.

Rae-Young Kim He received the B.S. and M.S. degrees from the Hanyang University, Seoul, Korea, in 1997 and 1999, respectively, and the Ph.D. degree from the Virginia Polytechnic Institute and State University, Blacks burg, VA, in 2009, all in electrical engineering. From 1999 to 2004, he was a Senior Researcher at the Hyosung Heavy Industry R&D Center, Seoul, Korea. In 2009, he was a Postdoctoral Researcher at National Semiconductor Corporation, working a smart home energy management system. Since 2010, he has been with the Hanyang University, Seoul, Korea, where he is currently an Assistant Professor in the Department of Electrical and Biomedical Engineering. His research interests include modeling and control of power converter systems, soft switching techniques, energy management systems in smart grid applications, power converter systems for renewable energies, and motor drive systems. Dr. Kim received a First Prize Paper Award in IAS 2007. Since 2009, He has been a Member of the IEEE Industry Applications Society (IAS) Industry Power Converters Committee, and also served as a Reviewer for the IEEE Transaction on Industrial Electronics and the IEEE Transaction on Industry Applications.

Dong-Seok Hyun He received the B.S. and M.S. degrees from Hanyang University, Seoul, Korea, in 1973 and 1978, respectively, and the Ph.D. degree from Seoul National University, Seoul, Korea, in 1986, all in electrical engineering. From 1976 to 1979, he was a Researcher with the Agency of Defense Development, Korea. From 1984 to 1985, he was a Research Associate in the Department of Electrical Engineering, University of Toledo, Toledo, OH, and from 1988 to 1989, he was a Visiting Professor in the Department of Electrical Engineering, Technical University of Munich, Germany. Since 1979, he has been with Hanyang University, where he is currently a Professor in the Department of Electrical Engineering. He is the author of more than 650 publications concerning electric machine design, high-power engineering, power electronics, and motor drives. His research interests include power electronics, motor drives, traction, and their control systems. Dr. Hyun is a member of the IEEE Power Electronics, Industrial Electronics, Industry Applications, and Electron Devices Societies. He is also a member of the Institution of Engineering and Technology, the Korean Institute of Power Electronics, and the Korean Institute of Electrical Engineers.